Advanced Single-Ion Conducting Block Copolymer Electrolyte for Safer and Less Costly Lithium–Metal Batteries

Xu Dong, Alexander Mayer, Zhen Chen, Stefano Passerini,* and Dominic Bresser*

ABSTRACT: **High-performance polymer electrolyte systems for lithium–metal batteries (LMBs) commonly contain a relatively high amount of fluorine to stabilize the electrode|electrolyte interfaces, particularly that with lithium metal. Herein, we report an advanced single-ion conducting polymer electrolyte that contains less fluorine in the backbone than previous systems, enabling a significant cost reduction, while still providing highly stable cycling of LMB cells containing $LiNi_{0.6}Co_{0.2}Mn_{0.2}O_2$ (NCM_{622}) and $LiNi_{0.8}Co_{0.1}Mn_{0.1}O_2$ (NCM_{811}) positive electrodes. Moreover, we show that the choice of the incorporated "molecular transporters", i.e., small molecules with high mobility and a high dielectric constant to facilitate the Li^+ transport, is essential for achieving high-performance LMB cells. In fact, the transition from pure ethylene carbonate to a mixture with propylene carbonate allows for an extended electrochemical stability toward oxidation and higher limiting current density, resulting in enhanced rate capability and cycling stability of Li||NCM cells—and the possibility to cycle these cells also at ambient temperature.**

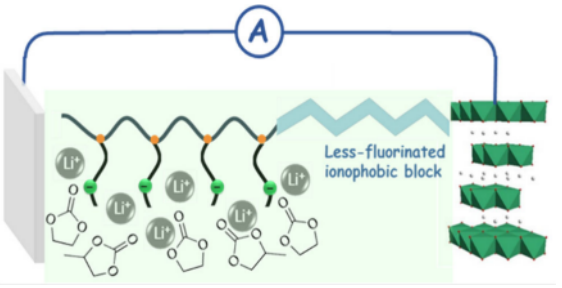

The continuously rising importance of lithium-ion batteries to power portable electronic devices and, more recently, electric vehicles has triggered great interest in lithium–metal batteries (LMBs), potentially offering an even higher energy density.[1−3] One of the great challenges toward a widespread commercialization of LMBs is the identification of a suitable electrolyte that enables long-term stable cycling and the formation of stable electrode|electrolyte interphases.[2,4−7] Given that electrolytes based on poly(ethylene oxide) (PEO) are presently the only commercial electrolyte system for LMBs,[8] polymers have attracted great attention in the past years owing to their suitable mechanical properties, thermal stability, and, not least, the proven commercial relevance of such systems.[4,9−18] For "classic" polymer electrolytes containing a dissolved lithium salt as, for instance, PEO, both ionic species are free to move. The polarization upon charge and discharge might results in severe concentration gradients of the ionic species within the cell, which may further result in an inhomogeneous, potentially dendritic, lithium deposition and the related safety issues.[19−23] Single-ion conducting polymer electrolytes (SIPEs), in which the anion is covalently tethered to the polymer backbone, may effectively solve this issue, as only the lithium cations are mobile.[24−29] Nonetheless, the high lithium-ion transference numbers (t_{Li}^+) of such systems is commonly accompanied by rather limited ionic conductivities at room temperature, frequently only about 10^{-7} to 10^{-5} S cm^{-1}.[30−32] The incorporation of organic carbonates with a high dielectric constant like ethylene carbonate (EC) or propylene carbonate (PC), however, can effectively enhance the conductivity of SIPEs at room temperature as these molecules may coordinate the lithium cations and facilitate the jump from one anionic site to another.[26,33−36] In this case, though, the mechanical properties of the ionomer may degrade, thus, requiring the blending with a second polymer such as polyvinylidene fluoride (PVdF) or the hexafluoropropylene copolymer (PVdF-HFP).[33,34,36,37]

We recently reported the synthesis and electrochemical characterization of a SIPE based on multiblock copoly(arylene ether sulfone), which comprises both a largely fluorinated, rigid ionophobic block and a weakly coordinating ionophilic block, delivering remarkable ionic conductivity and stable cycling of $Li||LiNi_{1-x-y}Co_xMn_yO_2$ cells.[29,38−40] The rigid ionophobic block provides sufficient mechanical stability to yield self-

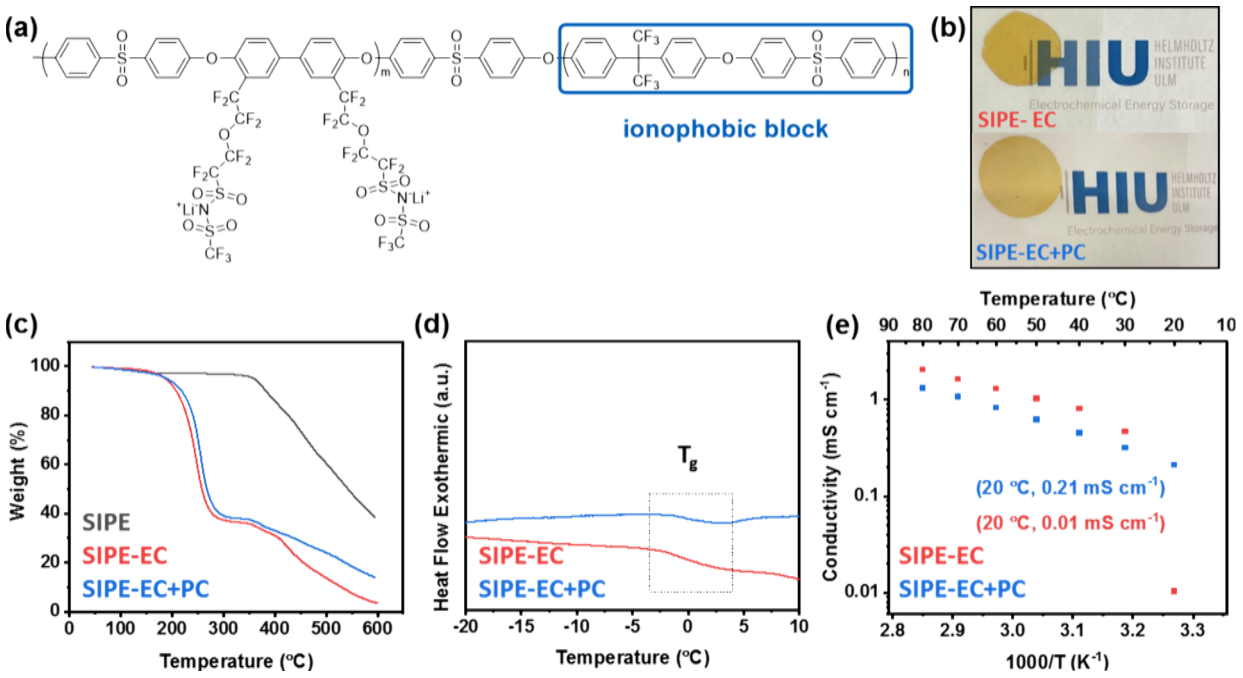

Figure 1. (a) Molecular structure of the new SIPE with an indication of the ionophobic block and an m/n ratio of 2/1. (b) Photographs of SIPE-EC (top) and SIPE-EC+PC (bottom). (c) TGA data recorded for the neat SIPE, SIPE-EC, and SIPE-EC+PC (sweep rate: 5 °C min^{-1}; atmosphere: O_2/N_2, 1:1). (d) DSC data recorded for SIPE-EC and SIPE-EC+PC with an indication of the glass transition temperature (T_g; heating rate: 5 °C min^{-1}). (e) Ionic conductivity as a function of temperature for SIPE-EC and SIPE-EC+PC with an indication of the ionic conductivity at 20 °C. The logo in Figure 1b is reproduced with permission from the Helmholtz Institute Ulm (HIU).

standing membranes, and the ionophilic block, selectively coordinating the small molecules with a high dielectric constant (also referred to as "molecular transporters"), provides fast Li^+ ion transport. The commonly rather high fluorine content in the ionophobic block, though, comes along with relatively high cost. Moreover, if pure EC is used as "molecular transporter", the system frequently requires operating temperatures of 40 °C and more due to the high melting point of EC (36 °C). Therefore, developing further enhanced SIPEs with a nonfluorinated or at least less-fluorinated ionophobic block and an optimized composition of the molecular transporters is important for the potential commercial use of these systems.

Accordingly, we synthesized a novel poly(arylene ether sulfone)-based single-ion conducting multiblock copolymer electrolyte, characterized by self-extinguishing properties (even if comprising generally flammable EC; see Video S1), with a less-fluorinated ionophobic block in the backbone, as depicted in Figure 1a. The synthesis of the SIPE with a reduced fluorine content and the basic characterization by nuclear magnetic resonance (NMR) spectroscopy (Figures S1–S3), Fourier transform infrared (FT-IR) spectroscopy (Figure S4), and gel permeation chromatography (GPC; Table S1) is described in the Supporting Information. Based on the precursors' cost for the herein developed SIPE and the earlier reported one,[29] a decrease in cost by 48% (Table S2) is anticipated, with a potential further reduction upon further optimization of the SIPE chemistry and synthesis scale-up. In fact, the given cost comparison is based on rather small quantities to be acquired from a provider of research chemicals. Scaling up the synthesis of such monomers naturally comes with a reduction of cost, which is apparently true for all chemicals, i.e., the fluorinated and nonfluorinated or less fluorinated compounds. Nevertheless, the synthesis of fluorinated organic compounds always requires additional synthetic steps, which naturally adds cost, and the use of highly corrosive and hazardous HF at some point, which requires particular safety precautions, thus, adding cost as well.[41−44] Hence, it is anticipated that fluorine-free and fluorine-poorer monomers will be more cost-efficient than (highly) fluorinated ones also when synthesized at a larger scale.

To enhance, in a next step, also the ambient and low temperature performance, we evaluated the impact of the molecular transporters incorporated into the SIPE and compared pure EC with a 1:1 mixture of EC and PC, which combines the higher dielectric constant of EC[45] and the lower melting point of PC (−49 °C). The appearance of the membranes after swelling with 55 wt % of EC and EC+PC is shown in Figure 1b. Thermogravimetric analysis (TGA) of the neat SIPE, SIPE-EC, and SIPE-EC+PC is presented in Figure 1c. The comparison reveals that the neat SIPE is stable until 350 °C, while the swollen SIPEs show a mass loss of 55 wt % between 150 and 250 °C, which is ascribed to the evaporation of EC and EC+PC. Figure 1d shows the differential scanning calorimetry (DSC) data recorded for the two swollen SIPEs. Both electrolyte systems exhibit a very similar glass transition temperature (T_g) in the range of 0 °C, indicating that the T_g is essentially independent from the choice of the molecular transporter—at least for the two systems investigated herein. The comparison of the ionic conductivity reveals a somewhat higher conductivity for SIPE-EC at temperatures of 30 °C and higher (Figure 1e), with around 0.78 mS cm^{-1} and 0.45 mS cm^{-1} at 40 °C for SIPE-EC and SIPE-EC+PC, respectively, and more than 1 mS cm^{-1} at 70 °C for both electrolytes. At 20 °C, however, the ionic conductivity of SIPE-EC drops sharply to only 0.01 mS cm^{-1} at 20 °C owing to the solidification of EC, while it is 0.21 mS cm^{-1}, i.e., 20 times higher, for SIPE-EC+PC. To confirm the contribution of the solvent molecules to the charge transport, we exemplarily fitted the ionic conductivity data of SIPE-EC +PC with the Vogel−Fulcher−Tammann[46] (VFT) and the

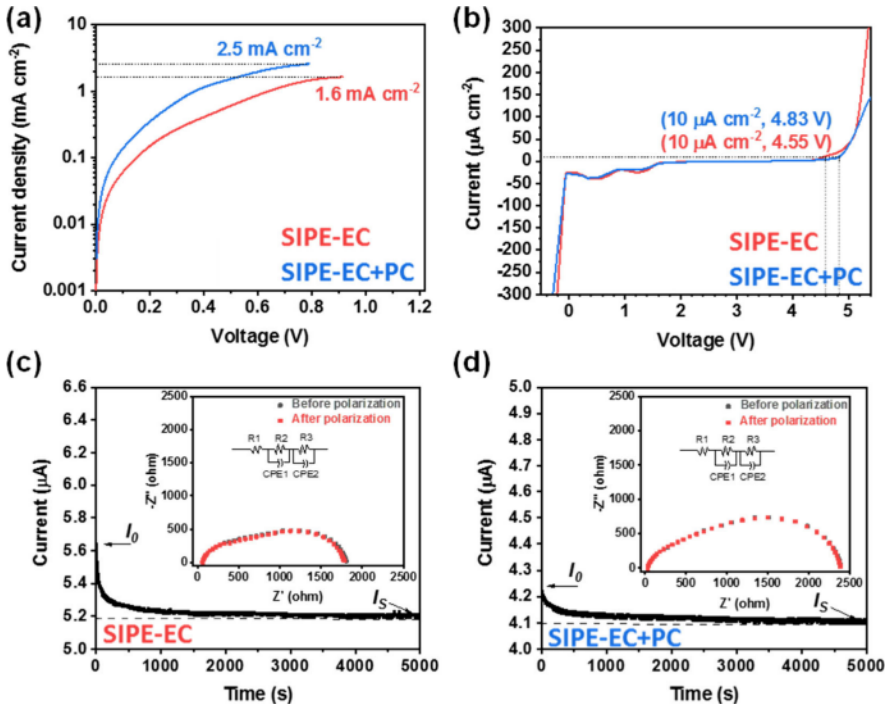

Figure 2. (a) **Determination of the limiting current density and (b) electrochemical stability window by linear sweep voltammetry of SIPE-EC and SIPE-EC+PC. (c,d) Determination of the lithium-ion transference number (t_{Li}^{+}) via a combination of chrononamperometry and electrochemical impedance spectroscopy (EIS) for (c) SIPE-EC and (d) SIPE-EC+PC; the equivalent circuits used for the analysis of the EIS data are provided as insets. All measurements were performed at 40 °C.**

Arrhenius equation (Figure S5). This comparison revealed that the use of the VFT equation yielded a substantially better fit, corroborating a solvent-coordinated Li^+ transport, supported by the enhanced mobility of the ionic side chains when coordinated by the solvent molecules.[29]

Figure 2a shows the determination of the limiting current density in symmetric Li||Li cells at 40 °C. In both cases, it is rather high with about 1.6 mA cm^{-2} for SIPE-EC and around 2.5 mA cm^{-2} for SIPE-EC+PC—both values being higher than the limiting current density of about 1.2 mA cm^{-2} recorded earlier for the first SIPE of this class.[29] The higher limiting current density of SIPE-EC+PC indicates that the charge transport in these systems is not solely reflected by the ionic conductivity. Beside the positive effect of PC on the limiting current density and the ambient ionic conductivity, the partial replacement of EC appears to have a beneficial impact also on the electrochemical stability toward oxidation as shown in the linear sweep voltammetry tests illustrated in Figure 2b. Setting the current threshold at 10 μA cm^{-2}, the anodic stability of SIPE-EC+PC (4.83 V) is slightly higher than that of SIPE-EC (4.55 V), which is ascribed to the higher anodic stability of PC compared to EC[47−49] and the resulting decomposition products propylene oxide and ethylene oxide, respectively.[50] Accordingly, we may anticipate that a further improvement of the electrochemical stability toward oxidation may be achieved by introducing suitable additives (potentially benefiting from the work conducted for liquid organic electrolytes[51,52]) and/or more oxidation-resistant molecular transporters (e.g., supported by computational studies, as they simultaneously need to provide a high dielectric constant and a sufficiently low melting point). For the cathodic sweep, there is essentially no difference for the two electrolyte systems—both being very stable, presumably owing to the formation of LiF at the interface with lithium metal.[53] Besides, some minor features at above and below 1.0 V, prior to the onset of lithium plating, are assigned to the reaction with the native NiO surface layer on the nickel electrodes and the solvent decomposition, respectively.[29,54,55]

To complete the basic electrochemical characterization of the two electrolyte systems, we determined the lithium-ion transference number using the method reported by Bruce, Vincent and Evans,[56,57] combining a potentiostatic measurement with electrochemical impedance spectroscopy (EIS). The results are presented in Figure 2c,d (see the Supporting Information for the experimental details), revealing a lithium-ion transference number of 0.93 and 0.94 for SIPE-EC and SIPE-EC+PC, respectively, which is fairly close to unity. Such a minor deviation is frequently observed for SIPEs,[58−60] and presumably results from a spontaneous formation of an interphase at the electrodelelectrolyte interface and the charge transport across this interphase.[61]

The compatibility with lithium metal was further investigated by lithium stripping/plating experiments in symmetric Li||Li cells at 40 °C (Figure 3). When applying a constant current density of 0.01 mA cm^{-2} (Figure 3a), both electrolyte systems show a rather comparable overpotential, which slightly increases initially before stabilizing after about 60−70 h. The overpotential remains a little lower, though, for SIPE-EC+PC and constant for 400 h, while there is a slight increase toward the end for SIPE-EC, indicating that PC contributes to the establishment of a more stable interphase. The more favorable interfacial stability and charge transport becomes even more apparent when varying the current density from 0.005 mA cm^{-2} to 0.5 mA cm^{-2} (with 20 stripping/plating cycles at each current density; Figure 3b). Again, both electrolyte systems provide rather stable overpotentials, which scale with the current density. The magnification of selected lithium stripping/plating cycles

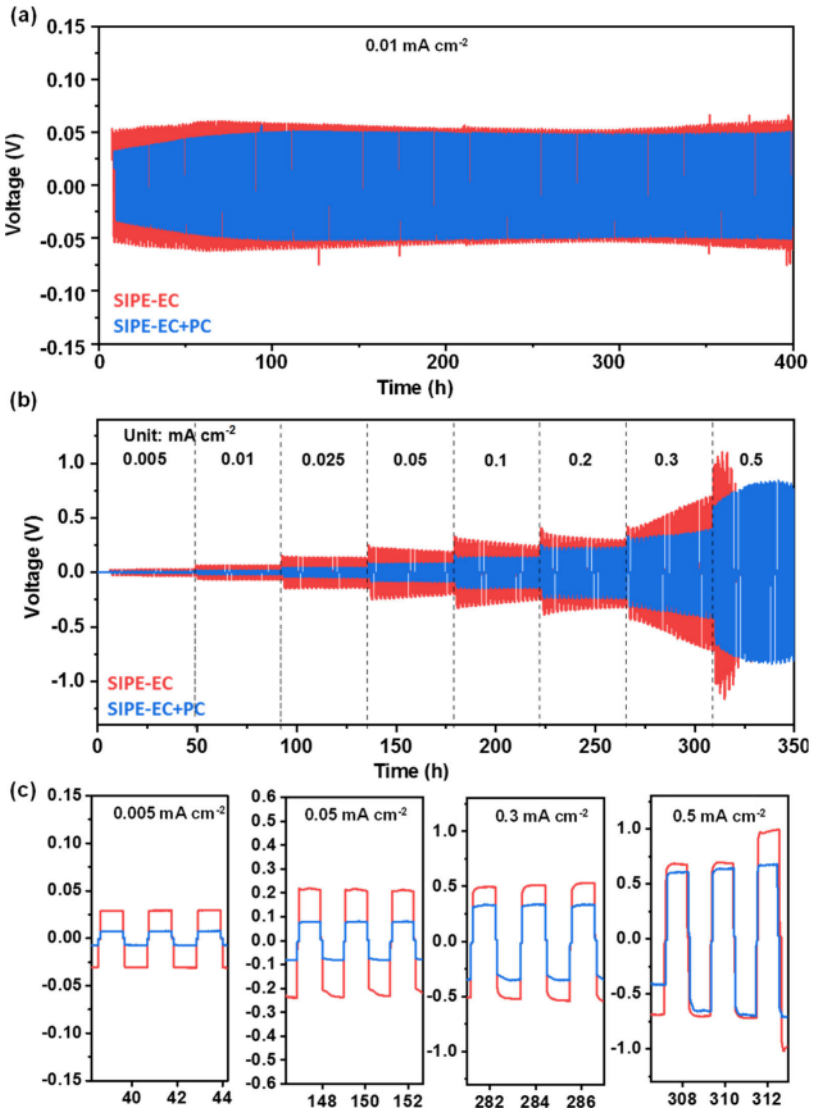

Figure 3. Lithium stripping/plating tests conducted on symmetric Li||Li cells employing SIPE-EC and SIPE-EC+PC as the electrolyte at (a) 0.01 mA cm^{-2} (areal capacity: 0.01 mAh cm^{-2}) and (b) varying current densities, ranging from 0.005 to 0.5 mA cm^{-2} (areal capacity: 0.005 to 0.5 mAh cm^{-2}), with (c) a magnification of selected lithium stripping/plating cycles at different current densities (T = 40 °C, each stripping and plating step lasted for 1 h).

shows essentially constant voltage responses (Figure 3c), as expected for a single-ion conductor.[62,63] However, the cells employing SIPE-EC+PC show generally a lower overpotential than the ones containing SIPE-EC. For instance, at 0.1 mA cm^{-2} the initial overpotential of the SIPE-EC+PC cell (0.13 V) is only half that of the SIPE-EC cell (0.25 V), underlining the beneficial impact of PC on the interfacial charge transfer. At elevated current densities of 0.3 mA cm^{-2}, SIPE-EC shows a steadily increasing overpotential, before finally suffering from a short circuit at 0.5 mA cm^{-2}. In contrast, the overpotential remains rather stable for SIPE-EC+PC at 0.3 mA cm^{-2} and does not show any sign of a short circuit at 0.5 mA cm^{-2}, despite an initial increase in polarization before it stabilizes. In sum, the presence of PC appears favorable for the interfacial stability and charge transport.

In a next step, we studied the two electrolyte systems in Li||NCM$_{622}$ cells (Figure 4), starting with an evaluation of the rate capability at 40 °C (Figure 4a). While the specific capacity is basically the same for both electrolytes, it drops much faster for SIPE-EC, providing only about 20 mAh g^{-1} at 1C, while it is still around 106 mAh g^{-1} for SIPE-EC+PC. The comparison of the corresponding dis-/charge profiles, depicted in Figure 4b, reveals that this greater capacity loss at elevated C rates originates from a much higher polarization. These findings further highlight the beneficial impact of PC on the interfacial charge transport and, with regard to the slightly higher stability toward oxidation (Figure 2b), maybe also at the cathode/electrolyte interface. Similarly, the constant current cycling at an intermediate C rate (0.2C) shows a higher capacity retention for SIPE-EC+PC (87.4%) compared to SIPE-EC (82.3%) after 300 cycles (Figure 4c). The comparison of the corresponding dis-/charge profiles (Figure 4d) suggests that this is largely related to a shortening of the dis-/charge profiles, indicating either a less stable interface with the positive electrode or an inferior wetting and consequent contact loss at the porous positive electrode. When decreasing the ambient temperature to 20 °C (Figure 4e), the specific capacity of the SIPE-EC cells rapidly drops—presumably owing to the solidification of EC, accompanied by a substantial decrease in ionic conductivity and contact loss—while the SIPE-EC+PC cells provide a very stable cycling at 0.3C

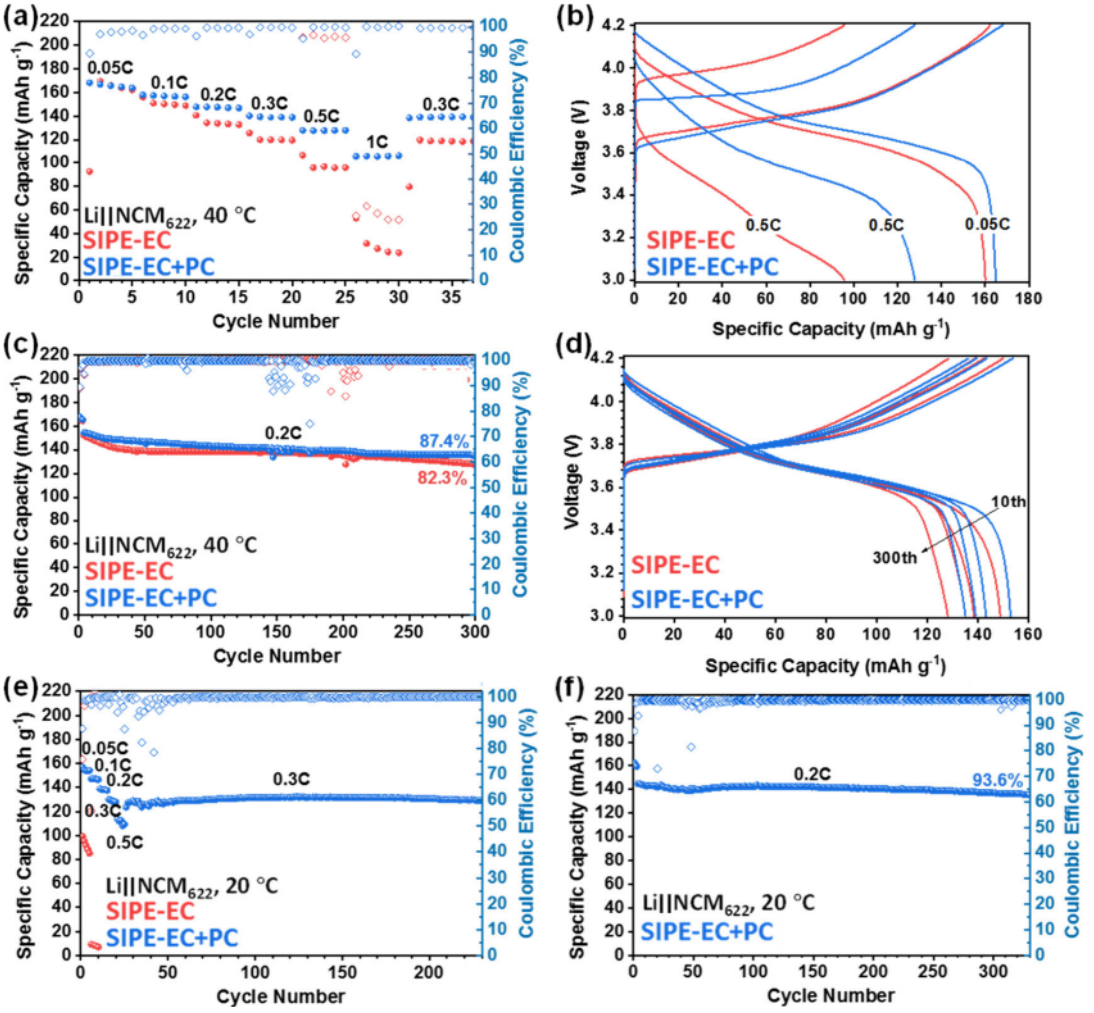

Figure 4. Comparison of the performance of Li||NCM$_{622}$ cells employing SIPE-EC and SIPE-EC+PC as the electrolyte: (a) evaluation of the rate capability at C rates ranging from 0.05C to 1C (T = 40 °C); (b) selected dis-/charge profiles obtained at the different C rates; (c) plot of the specific discharge capacity upon long-term constant current cycling at 0.2C (i.e., 0.08 mA cm^{-2}) with an indication of the eventual capacity retention for both electrolytes (T = 40 °C); (d) selected dis-/charge profiles at 0.2C from the 1st to the 300th cycle; (e) evaluation of the rate capability at C rates ranging from 0.05C to 0.5C, followed by constant current cycling at 0.3C with an indication of the average Coulombic efficiency for SIPE-EC+PC (T = 20 °C); (f) plot of the specific discharge capacity upon long-term constant current cycling at 0.2C (i.e., 0.08 mA cm^{-2}) for SIPE-EC+PC with an indication of the average Coulombic efficiency and eventual capacity retention (T = 20 °C). All tests were performed with cutoff voltages of 3.0 and 4.2 V.

and reasonable rate capability with about 160 mAh g^{-1} at 0.05C and around 106 mAh g^{-1} at 0.5C (i.e., 0.2 mA cm^{-2}; see also Figure S6), thus, further underlining the beneficial impact of the presence of "low-melting" PC. Additional tests at 0.2C (Figure 4f) show that the capacity retention after more than 300 cycles remained very high with about 93.6%, which originates (among others) from the rather high average Coulombic efficiency of 99.5% and is at least competitive, if not superior to previous studies employing NCM-type cathodes (Table S3).

To further investigate the suitability of our electrolyte system with state-of-the-art lithium-ion positive electrode materials, we assembled Li||NCM$_{811}$ cells and subjected them to galvanostatic cycling experiments (Figure 5). The cells containing either SIPE-EC or SIPE-EC+PC show a very similar capacity during the first cycle at 0.05C (Figure 5a). However, when elevating the C rate, the capacity of the Li|SIPE-EC|NCM$_{811}$ cell drops faster than the capacity of the Li|SIPE-EC+PC|NCM$_{811}$ cell. At 2C, the latter cell shows a rather high discharge capacity (109 mAh g^{-1}) while the capacity of the former drops to about 62 mAh g^{-1}. This superior performance is attributed to the better interfacial contact in the presence of PC, enabling a faster charge transfer, as also indicated by a lower polarization at elevated C rates (Figure 5b). When subjecting the cells to constant current cycling at 0.2C (Figure 5c), the cells containing EC and EC+PC exhibit a high discharge capacity retention of 82.7% (137 mAh g^{-1}) and 75.9% (123 mAh g^{-1}), respectively, after 200 cycles. The comparison of the corresponding dis-/charge profiles (Figure 5d) shows a higher polarization for the cell containing SIPE-EC, supporting for a poorer interfacial contact and/or stability.

Following these very good results for SIPE-EC+PC, we increased the active material mass loading of the NCM$_{811}$ electrode by a factor of 4 to about 11.4 ± 0.1 mg cm^{-2} (including 5 wt % of the SIPE to ensure a suitable ionic conductivity) and increased the electrode size from about 1.13 cm^2 (disk shape) to 16 cm^2 (squared, 4 × 4 cm^2), assembled in pouch cells. These cells show a comparable specific capacity of 177 mAh g^{-1} at 0.05C (Figure 5e). When increasing the C rate

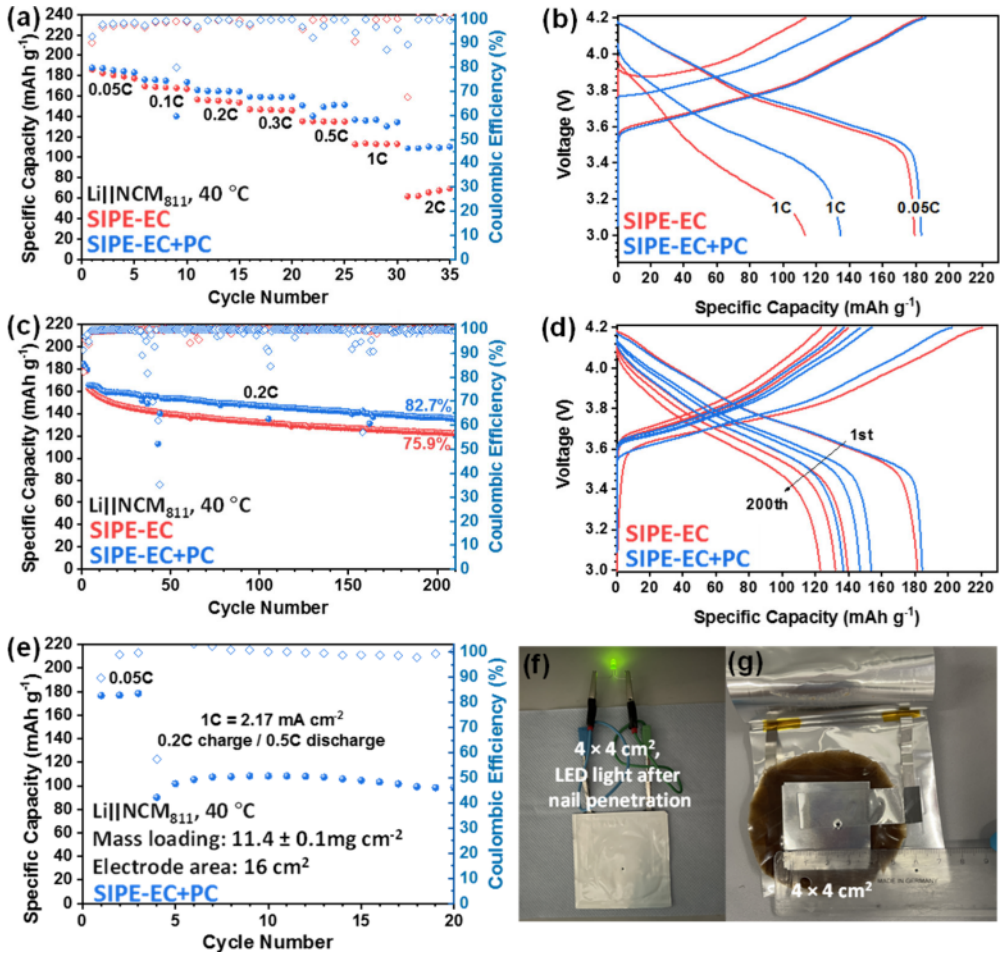

Figure 5. (a–d) Comparison of the performance of Li||NCM_{811} cells employing SIPE-EC and SIPE-EC+PC as the electrolyte: (a) evaluation of the rate capability at varying C rates, ranging from 0.05C to 2C (T = 40 °C); (b) selected dis-/charge profiles obtained at the different C rates; (c) plot of the specific discharge capacity upon long-term constant current cycling at 0.2C (i.e., 0.11 mA cm^{-2}) with an indication of the average Coulombic efficiency and eventual capacity retention for both electrolytes (T = 40 °C); (d) selected dis-/charge profiles at 0.2C from the 1st to the 200th cycle. (e) Galvanostatic cycling of Li|SIPE-EC+PC|NCM_{811} cells at 0.2C/0.5C (charge/discharge), employing NCM_{811} cathodes with a high active material mass loading of 11.4 ± 0.1 mg cm^{-2} and an electrode area of 4 × 4 cm^2 (T = 40 °C). All tests were performed within the cutoff voltages of 3.0 and 4.2 V. (f) Photograph of the 4 × 4 cm^2 Li||NCM_{811} cells lighting a green LED after the nail penetration experiment and (g) photograph of a disassembled 4 × 4 cm^2 Li||NCM_{811} cell from the back side of the NCM_{811} electrode after the nail penetration experiment.

to 0.2C and 0.5C for the charge and discharge step, respectively, though, the capacity decreases to about 90 mAh g^{-1}, indicating that further improvement of the electrode composition and architecture is needed. Nevertheless, the capacity remains stable for 20 cycles, underlining that the material as such is very well suited for this cell chemistry—even when increasing the cathode active material mass loading to commercially meaningful values—and, thus, to far higher values than commonly reported in the scientific literature (see Table S3). Anticipating further advances concerning the electrode composition and architecture, the "simple" implementation of the SIPE into the positive electrode, yielding "standard" electrode tapes, in combination with the self-standing properties of the SIPE membranes, owing to the presence of the ionophobic block, render a state-of-the-art roll-to-roll cell fabrication as used for commercially available LMBs feasible.

Finally, we evaluated the safety of this SIPE system. In a first step, we cut Li||NCM_{811} pouch cells containing SIPE-EC (Figure S7a) and SIPE-EC+PC (Figure S7b) in half, and both cells continued to power the blue LED light connected to the cells. Notably, the LED light powered by the Li||NCM_{811} containing SIPE-EC+PC appeared generally brighter—before and after the cut—being in line with the aforementioned greater performance of this electrolyte. In a second step, we subjected the Li||NCM_{811} cells comprising SIPE-EC+PC and the large electrodes to a nail penetration test with a stainless-steel nail after charging the cell at 0.1C (i.e., 0.055 mA cm^{-2}) to 4.2 V. The cells got short-circuited when the nail was punched into the cell and, thus, electronically connected the two electrodes directly (Video S2). However, as soon as the nail was removed, the green LED started shining again (Video S2, Figure 5f, and Figure S7c), revealing that this short circuit did not have any significant impact on the cell. In fact, we repeated this nail penetration experiment thrice on the same cell and the observation was always the same: the cell got short-circuited when the nail was punched through the cell, but the LED started shining again as soon as the nail was removed (Video S2, Figure S7d–f), and there was no apparent heat evolution or any other indication of any significant degradation of the cell—as also evident from the magnification of the relevant area after opening the cell inside a glovebox (Figure 5g). These results, even if being rather

qualitative, nicely highlight the great safety features of these SIPE systems.

In summary, a new single-ion conducting multiblock copolymer electrolyte has been successfully synthesized, featuring a less-fluorinated ionophobic block and substantially reduced synthesis cost (based on an evaluation of the current lab-scale prices). The physicochemical and electrochemical characterization of these polymer electrolytes comprising different molecular transporters, i.e., pure EC or a mixture of EC and PC, revealed that the latter system provides a higher ionic conductivity at room temperature, a higher limiting current density and slightly higher electrochemical stability toward oxidation, enabling a very good rate capability and cycling stability in Li||NCM_{622} and Li||NCM_{811} cells—at 40 and 20 °C, and even when increasing the active material mass loading to 11.4 ± 0.1 mg cm^{-2} for larger 4 × 4 cm^2 electrodes. Moreover, these electrolyte systems appear very safe based on an extended (still qualitative) safety evaluation by cutting the cells in half and subjecting them to a repeated nail penetration testing, rendering this new SIPE a promising candidate for the realization of cost-efficient, high-performance, and high-safety room-temperature LMBs.

AUTHOR INFORMATION

Corresponding Authors

Stefano Passerini − *Helmholtz Institute Ulm (HIU), 89081 Ulm, Germany; Karlsruhe Institute of Technology (KIT), 76021 Karlsruhe, Germany; Austrian Institute of Technology (AIT), Center for Transportation Technologies, 1020 Wien, Austria;* orcid.org/0000-0002-6606-5304; Email: stefano.passerini@kit.edu

Dominic Bresser − *Helmholtz Institute Ulm (HIU), 89081 Ulm, Germany; Karlsruhe Institute of Technology (KIT), 76021 Karlsruhe, Germany;* orcid.org/0000-0001-6429-6048; Email: dominic.bresser@kit.edu

Authors

Xu Dong − *Helmholtz Institute Ulm (HIU), 89081 Ulm, Germany; Karlsruhe Institute of Technology (KIT), 76021 Karlsruhe, Germany*

Alexander Mayer − *Helmholtz Institute Ulm (HIU), 89081 Ulm, Germany; Karlsruhe Institute of Technology (KIT), 76021 Karlsruhe, Germany*

Zhen Chen − *Helmholtz Institute Ulm (HIU), 89081 Ulm, Germany; Karlsruhe Institute of Technology (KIT), 76021 Karlsruhe, Germany;* orcid.org/0000-0002-5199-0935

Notes

The authors declare no competing financial interest.

ACKNOWLEDGMENTS

The authors would like to acknowledge financial support by the Federal Ministry of Education and Research (BMBF) within the FestBatt project (03XP0175B) and the FB2-Poly project (03XP0429B), as well as the financial support by the Helmholtz Association.

REFERENCES

(1) Liu, B.; Zhang, J.-G.; Xu, W. *Advancing lithium metal batteries. Joule* **2018**, *2*, 833−845.

(2) Zeng, X.-X.; Yin, Y.-X.; Li, N.-W.; Du, W.-C.; Guo, Y.-G.; Wan, L.-J. Reshaping lithium plating/stripping behavior via bifunctional polymer electrolyte for room-temperature solid Li metal batteries. *J. Am. Chem. Soc.* **2016**, *138*, 15825−15828.

(3) Chen, S.; Niu, C.; Lee, H.; Li, Q.; Yu, L.; Xu, W.; Zhang, J.-G.; Dufek, E. J.; Whittingham, M. S.; Meng, S. Critical parameters for evaluating coin cells and pouch cells of rechargeable Li-metal batteries. *Joule* **2019**, *3*, 1094−1105.

(4) Kalhoff, J.; Eshetu, G. G.; Bresser, D.; Passerini, S. Safer electrolytes for lithium-ion batteries: state of the art and perspectives. *ChemSusChem* **2015**, *8*, 2154−2175.

(5) Tikekar, M. D.; Choudhury, S.; Tu, Z.; Archer, L. A. Design principles for electrolytes and interfaces for stable lithium-metal batteries. *Nat. Energy* **2016**, *1*, 1−7.

(6) Keller, M.; Varzi, A.; Passerini, S. Hybrid electrolytes for lithium metal batteries. *J. Power Sources* **2018**, *392*, 206−225.

(7) He, X.; Bresser, D.; Passerini, S.; Baakes, F.; Krewer, U.; Lopez, J.; Mallia, C. T.; Shao-Horn, Y.; Cekic-Laskovic, I.; Wiemers-Meyer, S. The passivity of lithium electrodes in liquid electrolytes for secondary batteries. *Nat. Rev. Mater.* **2021**, *6*, 1036−1052.

(8) Bresser, D.; Lyonnard, S.; Iojoiu, C.; Picard, L.; Passerini, S. Decoupling segmental relaxation and ionic conductivity for lithium-ion polymer electrolytes. *Mol. Syst. Des. Eng.* **2019**, *4*, 779−792.

(9) Zhang, Q.; Liu, K.; Ding, F.; Liu, X. Recent advances in solid polymer electrolytes for lithium batteries. *Nano Res.* **2017**, *10*, 4139−4174.

(10) Scrosati, B.; Vincent, C. A. Polymer electrolytes: the key to lithium polymer batteries. *MRS Bull.* **2000**, *25*, 28−30.

(11) Wright, P. V. Polymer electrolytes—the early days. *Electrochim. Acta* **1998**, *43*, 1137−1143.

(12) Di Noto, V.; Lavina, S.; Giffin, G. A.; Negro, E.; Scrosati, B. Polymer electrolytes: Present, past and future. *Electrochim. Acta* **2011**, *57*, 4−13.

(13) Armand, M.; Chabagno, J.; Duclot, M. Polyethers as solid electrolytes. *Fast Ion Transport in Solids* **1979**, *52*, 131−136.

(14) Stephan, A. M. Review on gel polymer electrolytes for lithium batteries. *Eur. Polym. J.* **2006**, *42*, 21−42.

(15) Fenton, D. Complexes of alkali metal ions with poly (ethylene oxide). *Polymer* **1973**, *14*, 589.

(16) Xiao, Z.; Zhou, B.; Wang, J.; Zuo, C.; He, D.; Xie, X.; Xue, Z. PEO-based electrolytes blended with star polymers with precisely imprinted polymeric pseudo-crown ether cavities for alkali metal ion batteries. *J. Membr. Sci.* **2019**, *576*, 182−189.

(17) Wang, Y.-J.; Kim, D. PEGDA/PVdF/F127 gel type polymer electrolyte membranes for lithium secondary batteries. *J. Power Sources* **2007**, *166*, 202−210.

(18) Shen, W.; Li, K.; Lv, Y.; Xu, T.; Wei, D.; Liu, Z. Highly-safe and ultra-stable all-flexible gel polymer lithium ion batteries aiming for scalable applications. *Adv. Energy Mater.* **2020**, *10*, 1904281.

(19) Stephan, A. M.; Nahm, K. Review on composite polymer electrolytes for lithium batteries. *Polymer* **2006**, *47*, 5952−5964.

(20) Zhou, D.; Shanmukaraj, D.; Tkacheva, A.; Armand, M.; Wang, G. Polymer electrolytes for lithium-based batteries: advances and prospects. *Chem.* **2019**, *5*, 2326−2352.
(21) Armand, M. Polymers with ionic conductivity. *Adv. Mater.* **1990**, *2*, 278−286.
(22) Brissot, C.; Rosso, M.; Chazalviel, J.-N.; Lascaud, S. Dendritic growth mechanisms in lithium/polymer cells. *J. Power Sources* **1999**, *81*, 925−929.
(23) Doyle, M.; Fuller, T. F.; Newman, J. The importance of the lithium ion transference number in lithium/polymer cells. *Electrochim. Acta* **1994**, *39*, 2073−2081.
(24) Porcarelli, L.; Shaplov, A. S.; Salsamendi, M.; Nair, J. R.; Vygodskii, Y. S.; Mecerreyes, D.; Gerbaldi, C. Single-ion block copoly (ionic liquid) s as electrolytes for all-solid state lithium batteries. *ACS Appl. Mater. Interfaces* **2016**, *8*, 10350−10359.
(25) Hallinan, D. T., Jr; Balsara, N. P. Polymer electrolytes. *Annu. Rev. Mater. Res.* **2013**, *43*, 503−525.
(26) Liang, H.-P.; Bresser, D. Toward a mature charge transport: Lithium cations as solo travelers in advanced polymer electrolytes. *Matter* **2022**, *5*, 2436−2439.
(27) Dong, X.; Chen, Z.; Gao, X.; Mayer, A.; Liang, H.-P.; Passerini, S.; Bresser, D. Stepwise optimization of single-ion conducting polymer electrolytes for high-performance lithium-metal batteries. *J. Energy Chem.* **2023**, *80*, 174−181.
(28) Dong, X.; Bresser, D. Comprehension-driven design of advanced multi-block single-ion conducting polymer electrolytes for high-performance lithium-metal batteries. *J. Energy Chem.* **2024**, *94*, 357−359.
(29) Nguyen, H. D.; Kim, G. T.; Shi, J.; Paillard, E.; Judeinstein, P.; Lyonnard, S.; Bresser, D.; Iojoiu, C. J. E.; Science, E. Nanostructured multi-block copolymer single-ion conductors for safer high-performance lithium batteries. *Energy Environ. Sci.* **2018**, *11*, 3298−3309.
(30) Zhang, H.; Li, C.; Piszcz, M.; Coya, E.; Rojo, T.; Rodriguez-Martinez, L. M.; Armand, M.; Zhou, Z. Single lithium-ion conducting solid polymer electrolytes: advances and perspectives. *Chem. Soc. Rev.* **2017**, *46*, 797−815.
(31) Bouchet, R.; Maria, S.; Meziane, R.; Aboulaich, A.; Lienafa, L.; Bonnet, J.; Phan, T. N. T.; Bertin, D.; Gigmes, D.; Devaux, D. Single-ion BAB triblock copolymers as highly efficient electrolytes for lithium-metal batteries. *Nat. Mater.* **2013**, *12*, 452−457.
(32) Porcarelli, L.; Shaplov, A. S.; Bella, F.; Nair, J. R.; Mecerreyes, D.; Gerbaldi, C. Single-ion conducting polymer electrolytes for lithium metal polymer batteries that operate at ambient temperature. *ACS Energy Lett.* **2016**, *1*, 678−682.
(33) Bresser, D.; Lyonnard, S.; Iojoiu, C.; Picard, L.; Passerini, S. Decoupling segmental relaxation and ionic conductivity for lithium-ion polymer electrolytes. *Mol. Syst. Des. Eng.* **2019**, *4*, 779−792.
(34) Rohan, R.; Sun, Y.; Cai, W.; Zhang, Y.; Pareek, K.; Xu, G.; Cheng, H. Functionalized polystyrene based single ion conducting gel polymer electrolyte for lithium batteries. *Solid State Ion.* **2014**, *268*, 294−299.
(35) Oh, H.; Xu, K.; Yoo, H. D.; Kim, D. S.; Chanthad, C.; Yang, G.; Jin, J.; Ayhan, I. A.; Oh, S. M.; Wang, Q. Poly (arylene ether)-based single-ion conductors for lithium-ion batteries. *Chem. Mater.* **2016**, *28*, 188−196.
(36) Li, C.; Qin, B.; Zhang, Y.; Varzi, A.; Passerini, S.; Wang, J.; Dong, J.; Zeng, D.; Liu, Z.; Cheng, H. Lithium Batteries: Single-Ion Conducting Electrolyte Based on Electrospun Nanofibers for High-Performance Lithium Batteries. *Adv. Energy Mater.* **2019**, *9*, 1970029.
(37) Rohan, R.; Pareek, K.; Chen, Z.; Cai, W.; Zhang, Y.; Xu, G.; Gao, Z.; Cheng, H. A high performance polysiloxane-based single ion conducting polymeric electrolyte membrane for application in lithium ion batteries. *J. Mater. Chem. A* **2015**, *3*, 20267−20276.
(38) Steinle, D.; Chen, Z.; Nguyen, H.-D.; Kuenzel, M.; Iojoiu, C.; Passerini, S.; Bresser, D. Single-ion conducting polymer electrolyte for Li‖LiNi0.6Mn0.2Co0.2O2 batteries—impact of the anodic cutoff voltage and ambient temperature. *J. Solid State Electrochem.* **2022**, *26*, 97−102.
(39) Chen, Z.; Steinle, D.; Nguyen, H.-D.; Kim, J.-K.; Mayer, A.; Shi, J.; Paillard, E.; Iojoiu, C.; Passerini, S.; Bresser, D. High-energy lithium batteries based on single-ion conducting polymer electrolytes and Li[Ni0.8Co0.1Mn0.1]O2 cathodes. *Nano Energy* **2020**, *77*, 105129.
(40) Shi, J.; Nguyen, H.-D.; Chen, Z.; Steinle, D.; Barnsley, L.; Li, J.; Frielinghaus, H.; Bresser, D.; Iojoiu, C.; Paillard, E. Nanostructured block copolymer single-ion conductors for low-temperature, high-voltage and fast charging lithium-metal batteries. *Energy Mater.* **2023**, *3*, 300036.
(41) Dolbier, W. R., Jr Fluorine chemistry at the millennium. *J. Fluor. Chem.* **2005**, *126*, 157−163.
(42) Lemal, D. M. Perspective on fluorocarbon chemistry. *J. Org. Chem.* **2004**, *69*, 1−11.
(43) Petkowski, J. J.; Seager, S.; Bains, W. Reasons why life on Earth rarely makes fluorine-containing compounds and their implications for the search for life beyond Earth. *Sci. Rep.* **2024**, *14*, 15575.
(44) Britton, R.; Gouverneur, V.; Lin, J. H.; Meanwell, M.; Hu, J. Contemporary synthetic strategies in organofluorine chemistry. *Nat. Rev. Method. Prime.* **2021**, *1*, 47.
(45) Silva, L. B.; Freitas, L. C. G. Structural and thermodynamic properties of liquid ethylene carbonate and propylene carbonate by Monte Carlo Simulations. *J. Mol. Struct.* **2007**, *806*, 23−34.
(46) Wang, L.; He, Y.; Xin, H. L. Transition from Vogel-Fulcher-Tammann to Arrhenius Ion-Conducting Behavior in Poly (Ethyl Acrylate)-Based Solid Polymer Electrolytes via Succinonitrile Plasticizer Addition. *J. Electrochem. Soc.* **2023**, *170*, No. 090525.
(47) Petibon, R.; Xia, J.; Ma, L.; Bauer, M. K.; Nelson, K. J.; Dahn, J. Electrolyte system for high voltage li-ion cells. *J. Electrochem. Soc.* **2016**, *163*, A2571.
(48) Ma, L.; Glazier, S.; Petibon, R.; Xia, J.; Peters, J. M.; Liu, Q.; Allen, J.; Doig, R.; Dahn, J. A guide to ethylene carbonate-free electrolyte making for Li-ion cells. *J. Electrochem. Soc.* **2017**, *164*, A5008.
(49) Metzger, M.; Marino, C.; Sicklinger, J.; Haering, D.; Gasteiger, H. A. Anodic oxidation of conductive carbon and ethylene carbonate in high-voltage Li-ion batteries quantified by on-line electrochemical mass spectrometry. *J. Electrochem. Soc.* **2015**, *162*, A1123.
(50) Arakawa, M.; Yamaki, J.-i. Anodic oxidation of propylene carbonate and ethylene carbonate on graphite electrodes. *J. Power Sources* **1995**, *54*, 250−254.
(51) Guo, K.; Qi, S.; Wang, H.; Huang, J.; Wu, M.; Yang, Y.; Li, X.; Ren, Y.; Ma, J. High-Voltage Electrolyte Chemistry for Lithium Batteries. *Small Sci.* **2022**, *2*, 2100107.
(52) Tan, S.; Ji, Y. J.; Zhang, Z. R.; Yang, Y. Recent Progress in Research on High-Voltage Electrolytes for Lithium-Ion Batteries. *ChemPhysChem* **2014**, *15*, 1956−1969.
(53) Mayer, A.; Nguyen, H. D.; Mariani, A.; Diemant, T.; Lyonnard, S.; Iojoiu, C.; Passerini, S.; Bresser, D. Influence of Polymer Backbone Fluorination on the Electrochemical Behavior of Single-Ion Conducting Multiblock Copolymer Electrolytes. *ACS Macro Lett.* **2022**, *11*, 982−990.
(54) Yamada, Y.; Takazawa, Y.; Miyazaki, K.; Abe, T. Electrochemical lithium intercalation into graphite in dimethyl sulfoxide-based electrolytes: effect of solvation structure of lithium ion. *J. Phys. Chem. C* **2010**, *114*, 11680−11685.
(55) Zhang, X.; Kostecki, R.; Richardson, T. J.; Pugh, J. K.; Ross, P. N. Electrochemical and infrared studies of the reduction of organic carbonates. *J. Electrochem. Soc.* **2001**, *148*, A1341.
(56) Evans, J.; Vincent, C. A.; Bruce, P. G. Electrochemical measurement of transference numbers in polymer electrolytes. *Polymer* **1987**, *28*, 2324−2328.
(57) Bruce, P. G.; Evans, J.; Vincent, C. A. Conductivity and transference number measurements on polymer electrolytes. *Solid State Ion.* **1988**, *28*, 918−922.
(58) Zhang, J.; Wang, S.; Han, D.; Xiao, M.; Sun, L.; Meng, Y. Lithium (4-styrenesulfonyl)(trifluoromethanesulfonyl) imide based single-ion polymer electrolyte with superior battery performance. *Energy Storage Mater.* **2020**, *24*, 579−587.
(59) Wang, Y.; Sun, Q.; Zou, J.; Zheng, Y.; Li, J.; Zheng, M.; Liu, Y.; Liang, Y. Simultaneous High Ionic Conductivity and Lithium-Ion Transference Number in Single-Ion Conductor Network Polymer

Enabling Fast-Charging Solid-State Lithium Battery. *Small* **2023**, *19*, 2303344.
(60) Hou, T.; Qian, Y.; Li, D.; Xu, B.; Huang, Z.; Liu, X.; Wang, H.; Jiang, B.; Xu, H.; Huang, Y. Electronegativity-Induced Single-Ion Conducting Polymer Electrolyte for Solid-State Lithium Batteries. *Energy Environ. Mater.* **2023**, *6*, No. e12428.
(61) Borzutzki, K.; Nair, J. R.; Winter, M.; Brunklaus, G. Does cell polarization matter in single-ion conducting electrolytes? *ACS Appl. Mater. Interfaces.* **2022**, *14*, 5211−5222.
(62) Liang, H. P.; Chen, Z.; Dong, X.; Zinkevich, T.; Indris, S.; Passerini, S.; Bresser, D. Photo-Cross-Linked Single-Ion Conducting Polymer Electrolyte for Lithium-Metal Batteries. *Macromol. Rapid Commun.* **2022**, *43*, 2100820.
(63) Dong, X.; Liu, X.; Li, H.; Passerini, S.; Bresser, D. Single-Ion Conducting Polymer Electrolyte for Superior Sodium-Metal Batteries. *Angew. Chem.* **2023**, *135*, No. e202308699.